Heat Transfer During CO_2 Hydrate Formation in a Continuous Flow Reactor

D. Yang,*,† L. A. Le,† R. J. Martinez,† R. P. Currier,*,† D. F. Spencer,‡ and G. Deppe§,⊥

Los Alamos National Laboratory, Los Alamos, New Mexico 87545, SIMTECHE, 13474 Tierra Heights Road, Redding, California 96003, Nexant, Inc., San Francisco, California 94105

Received December 10, 2007. Revised Manuscript Received February 29, 2008

Mixtures of CO_2 and argon, or helium, were used to continuously produce CO_2 hydrate slurries at high linear fluid velocities and high gas volume fractions. The impact of gas carrier, fluid velocity, and slurry loading on heat transfer processes were investigated using a tubular continuous flow reactor. Due to the high gas volume fraction, the thermal conductivity of the carrier gas was found to significantly impact the heat transfer rate on the process fluid side. The overall heat transfer coefficient from a He/CO_2 gas mixture was found to be at least 50% higher than that obtained from a comparable Ar/CO_2 mixture. High fluid velocity in the hydrate formation reactor resulted in effective interphase mixing and, thus, enhanced both mass and heat transfer between the gas, liquid, and solid phases. With vigorous mixing, hydrate formation kinetics were very favorable and hydrate formation became heat-transfer limited.

Introduction

Fossil fuels currently supply over 85% of the energy used in the United States and are responsible for roughly 90% of US greenhouse gas emissions.[1] Use of these fuels, especially coal, is expected to increase significantly in the first half of the 21st century. Future utilization of coal would benefit greatly by demonstrating the ability to achieve near-zero emissions in power plant applications. One promising technology for realizing this goal is based on the integrated gasifier combined cycle (IGCC) design.[2–5] IGCC is a process that can utilize coal in the following way. Rather than burning coal directly, the IGCC process converts coal into other chemical constituents using gasification. The synthesis gas (syngas) stream exiting the gasifier consists predominately of carbon monoxide, hydrogen, carbon dioxide, and a suite of lesser constituents such as hydrogen sulfide and trace gases. The syngas may then be reacted with steam over a catalyst to convert the carbon monoxide to carbon dioxide and hydrogen, according to the water−gas shift reaction. The resulting "shifted" syngas then consists of predominantly H_2 (60%) and CO_2 (37−39%) with the balance being the lesser components, predominately hydrogen sulfide. The unwanted byproducts are removed, or treated, prior to combustion of the hydrogen fuel. IGCC technology can also provide a basis for industrial-scale carbon sequestration—that is the capture, transport and injection of CO_2 into suitable geological formations. A key element in achieving sequestration objectives is the ability to efficiently and cost-effectively separate CO_2 from shifted synthesis gas and provide pipeline pressure gas for transport to sequestration sites.

SIMTECHE conceived and patented a low temperature hydrate-based process for removing CO_2 from shifted syngas products derived from coal or natural gas.[6,7] This process shows promise of achieving many of the performance objectives for high efficiency power production with carbon capture.[7,8] The SIMTECHE process makes use of the fact that high pressure operations are being designed into IGCC flow sheets, motivated by both gasifier and gas turbine performance considerations. These higher processing pressures can be exploited to remove the CO_2 (and hydrogen sulfide) at elevated pressures by forming clathrate-hydrate inclusion compounds. The H_2 does not readily form hydrates under these conditions,[6–12] thus providing a basis for separation. A primary advantage of using hydrates as a separation agent is that upon decomposition of the hydrates, elevated pressure CO_2 can be produced.[13,14] This is especially important if pipeline pressure CO_2 is required for disposal or

* Corresponding authors. Dali Yang. Tel.: 1-505-665-4054. E-mail address: dyang@lanl.gov. Robert Currier. Tel.: 1-505-665-3601. E-mail address: currier@lanl.gov.

† Los Alamos National Laboratory.

‡ SIMTECHE.

§ Nexant, Inc.

⊥ Present address: Chevron Corp., 100 Chevron Way, Richmond, CA 94802.

(1) Klara, S. M.; Srivastava, R. D. US-DOE integrated collaborative technology development program for CO2 separation and capture. *Environ. Progr.* **2002**, *21* (4), 247–253.

(2) Booras, G. S.; Smelser, S. C. An engineering and economic evaluation of CO2 removal from fossil-fuel-fired power plants. *Energy* **1991**, *16* (11/12), 1295–305.

(3) Hess, G. Incentives boost coal gasification. *Chem. Eng. News* **2006**, *84* (3), 22–24.

(4) Joshi, M. M.; Lee, S. G. Integrated gasification combined cycle. A review of IGCC technology. *Energy Sources* **1996**, *18* (5), 537–68.

(5) Smith, D. J. IGCC: the 21st century's answer for the clean burning of coal. *Power Eng.* **2000**, *104* (11), 53–8.

(6) Spencer, D. *Methods and system from selectively separating CO2 from a multicomponent gaseous stream.* U.S.A. Patent No. 6,797,039, 2004.

(7) Spencer, D. *Methods and system for selectivity separating CO2 from a multicomponent gaseous stream to product a high pressure CO2 product.* U.S.A. Patent No. 7,128,777, 2006.

(8) Morgan, J. J.; Blackwell, V. R.; Johnson, D. E.; Spencer, D. F.; North, W. J. Hydrate formation from gaseous CO2 and water. *Environ. Sci. Technol.* **1999**, *33* (9), 1448–1452.

(9) Brewer, P.; Friederich, G.; Peltzer, E. T.; Orr, F. M. J. Direct Experiments on the Ocean Disposal of Fossil Fuel CO2. *Science* **1999**, 284.

(10) Robinson, D. B.; Mehta, B. R. *J. Can. Petr. Technol.* **1971**, *10*, 33–35.

(11) Zhang, S.; Chen, G.; Ma, C.; Yang, L.; Guo, T. *J. Chem. Eng. Data* **2000**, *45*, 908–911.

(12) Sugahara, T.; Murayama, S.; Hashimoto, S.; Ohgaki, K. Phase equilibria for H2+CO2+H(2)O system containing gas hydrates. *Fluid Phase Equilib.* **2005**, *233* (2), 190–193.

10.1021/ef700749f CCC: $40.75
Published on Web 06/10/2008

for use in enhanced oil recovery.[7] Specifically, the ability to capture the CO_2 at elevated pressures greatly reduces the parasitic compression costs required to provide pipeline pressure CO_2. Many conventional separation processes (e.g., amine-based scrubbing) yield low pressure CO_2 gas following solvent regeneration and thus involve substantial parasitic energy losses associated with CO_2 compression.

The clathrate-hydrate compounds at the heart of the SIMTECHE process are icelike solids that can incorporate light hydrocarbon gases, such as methane, CO_2, and H_2S into their crystalline structure.[15] The clathrates are structured inclusion compounds, which may or may not, be based on water. The hydrates, in turn, are the water-based clathrates in which a dissolved gas molecule (the "guest") is captured within polyhedral cages of hydrogen bonded water molecules (the "host"). Three primary water host structures have been identified.[15] Structure I (sI) is a combination of stacked pentagonal dodecahedral and tetrakaidecahedral water cages. Structure II (sII) consists of pentagonal dodecahedral and hexakaidecahedral cages. The less common hydrate structure, known as sH, consists of pentagonal dodecahedral, irregular dodecahedral, and icosahedral water cavities. Hydrates have the capacity to store large amount of gas and thus have attracted attention recently as a potential means of disposing CO_2 in the deep sea.[16–21] As a result, the thermodynamic and kinetic mechanisms of water−CO_2−hydrate (sI) systems have been studied extensively.[12,21–28] However, only a few studies have been conducted to investigate the effect of mixing on hydrate formation.[29–31]

Spencer and co-workers demonstrated previously[8,32] that CO_2 gas and liquid water can form hydrates rapidly (in less than 1.0 s) when the phases are vigorously mixed. These results were subsequently verified at Los Alamos in a bench-scale flow system using H_2/CO_2, He/CO_2, and Ar/CO_2 mixtures.[14] In order to better understand the effects of fluid velocity and heat transfer in a continuous flow hydrate formation system, an engineering test module (ETM) was constructed at Los Alamos National Laboratory. The ETM was designed to achieve both hydrate nucleation and equilibrium conversion.[13] This continuous flow tubular hydrate production reactor (having up to a 23 m long tail tube of 0.8 cm i.d.) allowed experiments to be conducted over a wide range of operating conditions, including high gas-to-liquid ratios (gas volume fraction >85%) and high fluid velocity (>4 m/s). It has been verified that with vigorous interphase mixing, the hydrate formation rates are very fast (< a few seconds). The thermodynamic limit of CO_2 conversion to hydrate was also realized in the ETM system.[13] During the hydrate formation process, the process fluid transitioned from a two-phase (gas−liquid) flow regime into three-phase (gas−liquid−solid) flow. Simultaneously, the hydrate heat-of-formation (roughly 60 kJ/mol) had to be continuously removed to promote additional hydrate formation. Thus, effective heat removal from the multiphase mixture was recognized to be an important operational and design issue. In this study, we examined the heat transfer issues associated with hydrate formation in a tubular, continuous flow reactor.

Heat transfer between two fluid streams separated by a solid cylindrical tube is typically described by an overall heat transfer coefficient, U_i, representing the various resistances. When heat flows from the tube-side process fluid through the wall and into the shell-side coolant, the overall heat transfer coefficient can be written[33] as:

$$\frac{1}{U_i} = \frac{1}{h_{PF}} + \frac{D_i}{k_{W,eff}} + \frac{1}{h_C} \cdot \frac{D_i}{D_o} \quad \text{where} \quad \frac{1}{k_{W,eff}} = \frac{\ln(D_o/D_i)}{2k_W} \tag{1}$$

D_i is the inner diameter of the tube (cm), D_o is the outer diameter of the tail tube (cm), and h_{PF} and h_C denote heat transfer coefficients (W/cm^2 K) on the process fluid and the coolant side, respectively. Here, k_W is the thermal conductivity of the tube wall material (W/cm K), and $k_{W,eff}$ is the effective conductivity of the wall with a specified thickness (∼2.68 W/cm K for the stainless steel tube employed in this set of experiments). The individual resistances can be identified as

$$R_{PF} = \frac{1}{h_{PF}} \qquad R_{Wall} = \frac{D_i}{k_{W,eff}} \qquad R_C = \frac{1}{h_C} \cdot \frac{D_i}{D_o} \tag{2}$$

where R_{PF}, R_{Wall}, and R_C correspond to the resistances associated with transferring heat from the process fluids to the wall,

(13) Anderson, G.; et al. *The Engineering Test Module (ETM): Construction, Commissioning, and Initial Hydrate Production Experiments*; Los Alamos National Laboratory Report LA-UR-05-7377, Annual Progress Report Submitted to DOE/NETL, 2006.

(14) Anderson, G.; et al *Continuous Hydrate Production Using Bench-Scale Flow Reactors*; Los Alamos National Laboratory Report LA-UR-04-6957, Annual Progress Report Submitted to DOE/NETL, 2005.

(15) Sloan, E. D. *Clathrate Hydrates of Natural Gases*, 2nd ed.; Marcel Dekker, Inc.: New York, 1998.

(16) Saji, A.; Noda, H.; Tanii, T.; Kawata, H.; Takata, T.; Shoji, K.; Kitamura, H.; Kamata, T. Simulation on sedimentation of CO2 in deep sea. *Kagaku Kogaku Ronbunshu* **1996**, *22* (6), 1273–1280.

(17) Koide, H.; Takahashi, M.; Shindo, Y.; Tazaki, Y.; Iijima, M.; Ito, K.; Kimura, N.; Omata, K. Hydrate formation in sediments in the subseabed disposal of CO2. *Energy* **1997**, *22* (2−3), 279–283.

(18) Mori, Y. H. Comments on "Simulation of Sedimentation of CO2 in Deep Sea". *Kagaku Kogaku Ronbunshu* **1997**, *23* (5), 738–739.

(19) Brewer, P. G.; Peltzer, E. T.; Walz, P.; Aya, I.; Yamane, K.; Kojima, R.; Nakajima, Y.; Nakayama, N.; Haugan, P.; Johannessen, T. Deep ocean experiments with fossil fuel carbon dioxide: Creation and sensing of a controlled plume at 4 km depth. *J. Marine Res.* **2005**, *63* (1), 9–33.

(20) Park, Y.; Kim, D.-Y.; Lee, J.-W.; Huh, D. G.; Park, K.-P.; Lee, J. Y.; H., L. Sequestering carbon dioxide into complex structures of naturally occurring hydrates. *Proc. Natl. Acad. Sci.* **2006**, *103* (34), 12690–12694.

(21) Lee, S.; Liang, L. Y.; Riestenberg, D.; West, O. R.; Tsouris, C.; Adams, E. CO_2 hydrate composite for ocean carbon sequestration. *Environ. Sci. Technol.* **2003**, *37* (16), 3701–3708.

(22) Uchida, T. Physical property measurements on CO2 clathrate hydrates. Review of crystallography, hydration number, and mechanical properties. *Waste Manage.* **1997**, *17* (5−6), 343–352.

(23) Uchida, T.; Mae, S.; Kawabata, J. Experimental studies of formation and dissociation mechanisms of gas hydrates. In *Proceedings of the 32nd Intersociety Energy Conversion Engineering Conference (IECEC-97)*, Honolulu, Hi, July 27−August 2; A.I.C.H.E., 1997; pp2064−2069.

(24) Ohgaki, K.; Hamanaka, T. Phase-Behavior of CO2 Hydrate-Liquid CO2-H2O System at High Pressure. *Kagaku Kogaku Ronbunshu* **1995**, *21* (4), 800–803.

(25) Zatsepina, O. Y.; Buffett, B. A. Experimental study of the stability of CO2-hydrate in a porous medium. *Fluid Phase Equilib.* **2001**, *192* (1−2), 85–102.

(26) Kato, M.; Iida, T.; Mori, Y. H. Drop formation behaviour of a hydrate-forming liquid in a water stream. *J. Fluid Mech.* **2000**, *414*, 367–78.

(27) Uchida, T.; Ikeda, I. Y.; Takeya, S.; Ebinuma, T.; Nagao, J.; Narita, H. CO2 hydrate film formation at the boundary between CO2 and water: effects of temperature, pressure and additives on the formation rate. *J. Cryst. Growth* **2002**, *237*, 383–387.

(28) Henning, R.; Schultz, A.; Thieu, V.; Halpern, Y. Neutron diffraction studies of CO2 clathrate hydrate: Formation from deuterated ice. *J. Phys. Chem. A* **2000**, *104* (21), 5066–5071.

(29) Yamasaki, A.; Takano, S.; Fujii, M.; Yanagisawa, Y.; Tajima, H.; Kiyono, F. Formation and growth of CO2 hydrate particles in a fluidized bed reactor. *Abstr. Pap. Am. Chem. Soc.* **2003**, *225*, U852−U852.

(30) Yamasaki, A.; Teng, H.; Wakatsuki, M.; Yanagisawa, Y.; Yamada, K. CO2 hydrate formation in various hydrodynamic conditions. *Ann. N.Y. Acad. Sci.* **2000**, *912*, 235–245.

(31) Tajima, H.; Yamasaki, A.; Kiyono, F. Effects of mixing functions of static mixers on the formation of CO2 hydrate from the two-phase flow of liquid CO2 and water. *Energy Fuels* **2005**, *19* (6), 2364–2370.

(32) North, W. J.; Blackwell, V. R.; Morgan, J. J. Studies of CO2 hydrate formation and dissolution. *Environ. Sci. Technol.* **1998**, *32* (5), 676–681.

(33) Bird, B. R.; Stewart, W. E.; Lightfoot, E. N. *Transport Phenomena*; John Wiley & Sons: New York, 1960; pp 389−420.

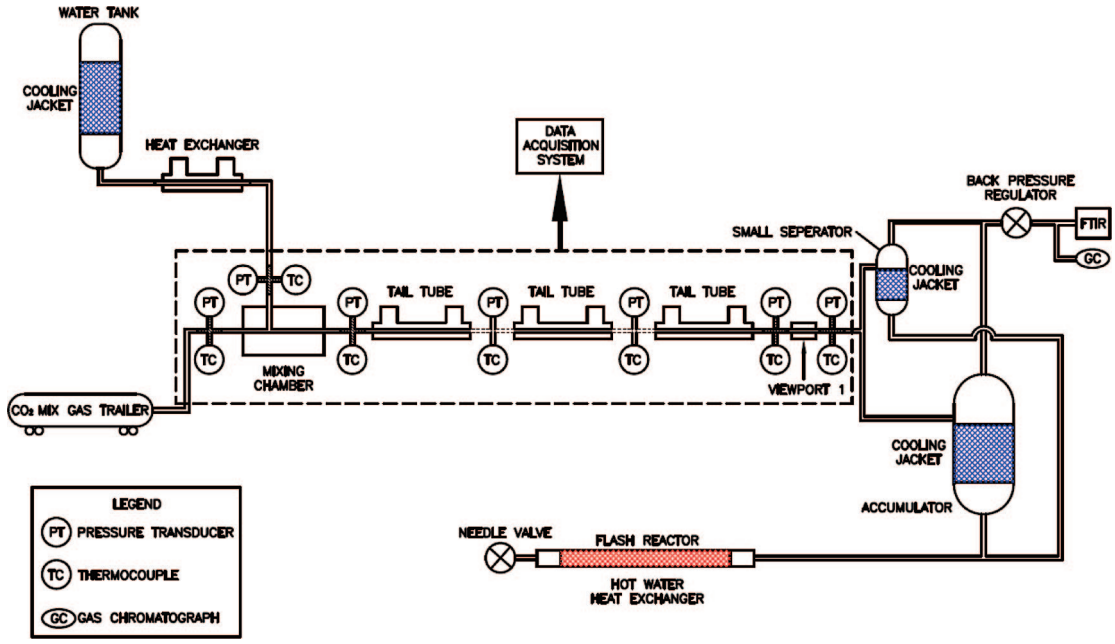

Figure 1. Schematic of the ETM system. Conceptually, the experiment is simple—water and gas are contacted (under hydrate forming conditions) in a venturi mixer and then passed down a horizontal finned tail tube heat exchanger which removes the hydrate heat-of-formation. The resulting hydrate slurry is then physically separated from the remaining gas and is then decomposed in a flash reactor.

conduction through the wall, and transferring from the tube wall to the shell-side coolant, respectively. The actual heat transfer rate depends on both flow conditions and on the physical properties of the fluids. Classical dimensional analysis[33] suggests heat transfer correlations of the form

$$Nu = Nu(Re, Pr, L/D_i)$$

$$Nu = \frac{D_i U_i}{k} \qquad Re = \frac{V_{PF} \rho D_i}{\mu} \qquad Pr = \frac{C_p \mu}{k} \qquad (3)$$

where Nu, Re, and Pr are Nusselt, Reynolds, and Prandlt numbers, respectively; k is the thermal conductivity (W/cm K), V_{PF} is the superficial velocity of process fluid (cm/s), ρ is the density (g/cm^3), μ is the viscosity of the fluid (cP), C_p is the heat capacity (J/g K), and L is the length of the tube (cm). Correlations of this form are often used to estimate heat transfer coefficients over a range of flow conditions.[33,34] However, for the process considered here, the correlation of heat transfer coefficients is not as straightforward. Ribbonlike metal fins are positioned throughout the coolant jacket to enhance heat transfer efficiency on the shell-side. The presence of the fins on the coolant side and the associated fin effectiveness complicates estimating the overall heat transfer coefficient. Although the shell-side coolant velocity is typically low in our experiments (<20 cm/s) and the resulting flow pattern is typically laminar, correlations for laminar flow cannot applied with confidence due to the presence of the ribbon fins. Therefore, a means of estimating the shell-side heat transfer coefficients is needed. In addition, on the tube-side where hydrate formation occurs, the flow changes from a two-phase (gas−liquid) regime to a three-phase regime (gas−liquid−solid) along the tail tube. The tube side is typically in turbulent flow (with Re > 100 000) which would result in an annular flow regime in a gas−liquid system gas volume fraction >85%. Thus, the empirical correlations developed for the two-phase annular and mist-annular flow conditions could be used to estimate the heat transfer coefficient at the early sections of the tail tube.[35] However, as a solid hydrate phase continually forms and increases in weight (and volume) fraction, the process fluid changes from what is initially a gas−liquid two phase flow into a gas−liquid−solid three phase flow along the tail tube. Thus, the gas−liquid correlations for heat transfer also become somewhat suspect if used in the downstream sections where considerable amounts of solid have formed. In the sections that follow, we outline an approach to estimating heat transfer parameters during continuous hydrate formation using thermal and material balances together with independent measurement of other thermal resistances.

Experimental Details

Continuous Flow Apparatus. A pictorial flowchart for the ETM flow system is shown in Figure 1. The ETM system consists of nine major components—gas delivery system, conditioned (i.e., CO_2 saturated) and raw water delivery systems, continuous flow reactor, chillers, small gas-slurry separator, accumulator, flash reactor for hydrate slurry decomposition, NDIR gas analyzer/sample collection stations, and data acquisition/instrument control system.

The central component in the ETM system is the continuous flow reactor (CFR). The CFR is essentially a tubular finned heat exchanger (referred to as the tail tube). The ETM design called for the tail tube to be comprised of individual sections of varying length, each of which can be independently cooled. This provided maximum flexibility in exploring the dynamics along the tail tube during hydrate formation. Tail tube sections were manufactured by Wieland-Werke AG (Germany) in lengths ranging from approximately 1 to 4 m. The exterior of the tubes consists of a dense, but irregular, array of copper ribbon fins that are brazed onto the outer tube wall. The results presented below on heat transfer dynamics are obtained from two specific ETM configurations. The first consisted of six tail tube sections (referred to as configuration one: sections A−F). Configuration two employed nine individual sections (sections D−L). Configuration one was ∼14.5 m long while configuration two was ∼22.5 m long. In both configurations, the inner diameter of the tail tube in which hydrate formation takes place is 0.8 cm. Each tail tube section had its own cooling jacket and flow meter to regulate coolant flow on the shell side.

(34) Hewitt, G.; Hall-Taylor, N. *Annular Two-Phase Flow*; Pergamon Press: New York, 1970.

(35) Davis, E. J.; David, M. M. 2-Phase Gas-Liquid Convection Heat Transfer. *Ind. Eng. Chem. Fundam.* **1964**, *3* (2), 111.

Temperature within each section was typically adjusted by varying the coolant flow rates. The coolant flow direction was countercurrent to the process fluid. Two polycarbonate view ports (LANL-made) were mounted along the tail tube to observe the multiphase flow pattern and verify the appearance of hydrates. The first view port was located in the upstream portion of the tail tube at a point where the incoming water and gas should be well mixed following contact in the venturi. The second view port was typically located at the exit of the tail tube just upstream of the separator/accumulator.

The two jacketed feedwater tanks (~180 L), a small separator (~10 L), and accumulator (~ 160 L) were actively cooled. A Mydax chiller system (model 1LH14A) with a capacity of 15 gal/min was dedicated to the CFR for temperature control. Several Thermo NesLab chillers (model HX300) were used to control coolant temperature for the water tanks, accumulator, and small separator, separately. The temperature of these units was controlled by adjusting the coolant temperature. The entire system was well insulated to minimize heat losses. Heat losses were quantified as discussed below.

NTC 2253Z thermistors (Advanced Thermal Products, Inc.) with accuracy ±0.1 °C and pressure transducers (PX613-3KG5V from Omega, Inc.) with accuracy ±2 psia were mounted before and after each tail tube section in the CFR to monitor the temperature and pressure. The tip of thermal sensors was carefully aligned with the bottom of the tail tube to ensure accurate measurement but not to significantly disturb the flow pattern within the CFR. Temperatures and pressures in other components of the ETM system (feed tanks, separator, accumulator, etc.) were also monitored and recorded. In all, the system was equipped with 19 pressure transducers and more than 60 thermal sensors (including thermistors and K-type thermocouples). As a backup, key pressure variables were also measured and displayed using mechanical Bourdon tube gauges visible from the operator station.

The water tanks and the accumulator were equipped with both a level (or volume) indicator (Drexel Brook, Inc.) and were placed upon a load cell balance (model 350 from GES, Inc.). High pressure coriolis mass flow meters (MFC 081 Smart from Krohne, Inc.) with accuracy ±0.1% were used to monitor the water flow rate at the entry and the gas flow rate at both the entry and exit of the CFR. Mass flow meter readouts were cross-referenced with the changes measured on the load cell (weight balance) in closing the material balance.

An NDIR gas analyzer (7300 series from Teledyne Analytical Instruments) was mounted to sample the off-gas stream and to provide an in situ measurement of CO_2 concentration. Gas samples were also periodically collected from the off-gas stream into gas sampler bottles. An HP M-series micro gas chromatograph (GC Model G2762A) was used to verify the CO_2 concentration. The chromatograph and NDIR were calibrated using certified Ar/CO_2 or He/CO_2 gas mixtures (Tri-Gas, Inc.). The agreement between these two measurements (NDIR analyzer and GC) was typically within ±1%.

Several data aquisition (DAQ) boards (model NI-4351 or NI-4350 from National Instruments) were used to convert analog readings into digital signals. The National Instruments LabView software program was used to communicate with the DAQ board to set and control operating conditions. The same LabView program also recorded all operating parameters during the course of an experiment. The sampling time interval was 20–40 s.

The ETM was designed for a maximum allowable working pressure of 1500 psia and was equipped with numerous pressure safety devices (pressure relief valves and rupture discs). The system was regularly leak-checked at 1500 psia prior to initiating hydrate experiments.

All process gases were purchased from Tri-Gas, Inc. The CO_2 mole fraction in the Ar/CO_2 and He/CO_2 mixtures ranged from 38~44%. Pure CO_2 (>99.99%) was used to prepare CO_2-saturated water for the hydrate experiments (also referred to as "conditioned" water). Pure N_2 (>99.99%) was used to conduct the calorimetric experiments to quantify heat losses. The coolant fluid was 30% ethylene glycol (Aldrich) in aqueous solution.

Experimental Procedures. Calorimetric experiments were carried out first to quantify heat exchange from the CFR to the ambient surroundings. The reactor tube was dried and purged using pure N_2 at ambient conditions and was then isolated from the remainder of the ETM system components. A series of experiments were performed in which the system was cooled using various coolant flow rates and coolant temperatures. Specifically, coolant flow rates ranging from 1.5 to 20 cm/s and inlet temperature settings ranging from −5 to 0 °C were used. Temperature changes in the coolant were carefully measured at steady state. A heat balance was used to estimate the heat gained by the coolant, due to convection between the CFR and surrounding environment and to conduction through the insulation. The quantitative estimates of heat gained by the coolant were taken into account when closing the energy balance in subsequent experiments.

To estimate the heat transfer coefficient on the ribbon-finned coolant side, thermal measurements were made using tube-side multiphase flow conditions similar to that used in the hydrate production. A nitrogen−water mixture was used at gas/liquid flow ratios similar to the hydrate formation runs (linear velocity >4 m/s, the gas volume fraction >70%). This mixture resulted in multiphase (gas−liquid) flow but avoided the heat generation associated with hydrate production. The water flow rate was controlled at 1500 g/min while the N_2 flow rate was controlled over the range of 110 to 400 g/min to mimic flow patterns observed during hydrate production. The coolant flow rate varied from 1.5 to 15 cm/s while the coolant temperature was set at ~0 °C in each section. To ensure that water did not freeze inside the tail tube, the inlet temperature of both water and N_2 was at ambient. The inlet pressure of N_2 gas was maintained at less than 150 psia. Using the "Wilson plot" method (described below), the heat transfer coefficient on the ribbon-finned coolant side was then estimated.

Prior to initiating a hydrate producing experiment, the feedwater was presaturated with CO_2 creating so-called "conditioned" water. To prepare conditioned water, a predetermined amount of pure CO_2 was metered into ~150 L of chilled water in the feed tank. The water within the tank was circulated from bottom to top to promote rapid saturation for more than 3 h to ensure completed saturation. The feed tank water was typically at a temperature of 2−4 °C. The reason for using conditioned water as the feed was to simulate recycle of process water. In the SIMTECHE process, water is recycled back to the hydrate formation reactor following hydrate dissociation. That recycled water will typically be saturated with CO_2 prior to re-entry into the reactor. In preparing conditioned water, the CO_2 solubility was determined using published solubility data.[36] At the time of use, the feed tank was overpressurized with nitrogen gas to deliver water into the CFR at the desired pressure (typically 800−1350 psia). The pressure at the exit of the CFR was maintained between 600−1100 psia. Depending on the operational conditions (e.g., CO_2 concentration, fluid velocity and slurry concentration), the pressure drop across the entire CFR ranged typically from 90−250 psia.

The feed gas, either Ar/CO_2 (CO_2 ~ 38−44%) or He/CO_2 (CO_2 ~ 39.0−42%), was delivered from either gas trailers or a gas cylinders. Pressurized water and gas were simultaneously jetted through a venturi at the inlet of the CFR. In the venturi, water was injected through the annular orifice as a dispersed phase into the gas phase (initially entering along the centerline). The gas served initially as the continuous phase. By adjusting the annular orifice, a well-mixed gas−liquid flow was produced. It was observed that the venturi orifice setting had some impact on initial hydrate nucleation; however, the overall performance of the system was not overly sensitive to the venturi settings. Turbulent fluid flow considerations suggest that after traveling approximately 30−50 tube diameters downstream, the flow pattern becomes governed by the hydrodynamics. In the ETM, a length/diameter (*L*/*D*) ratio of 50 is reached 0.4 m downstream of the venturi. Thus, over the 23 m length of the reactor, the initial mixing pattern provided by the

(36) Wender, I.; Sayari, A. *Chemistry and uses of carbon dioxide*; final report EPRI-AP-4631, Department of Chemical and Petroleum Engineering, Pittsburgh University: Pittsburgh, PA, 1986; p 119.

venturi proved to have relatively little impact on the overall performance of the system.

Downstream of the venturi, the process fluid temperature was controlled by adjusting the coolant flow rate in the individual tail tube sections. The exiting hydrate slurry and residual gas were sent into either a small separator or an accumulator where the liquid/hydrate phase was separated from the process fluid by gravity. The gas containing unreacted CO_2 was discharged from the top of these vessels. Finally, the slurry was pushed through a flash reactor, where heat was provided to decompose the hydrate.

Typical linear velocities of the process fluid (including gas, liquid, and hydrate) were larger than 4.0 m/s. The entry temperature of process fluid was typically less than 4.0 °C while the exit temperature of process fluid was also less than 4.0 °C. The coolant flow rate varied from one section to another, but was typically in the range from 1.3 to 7.2 kg/min. The water mass flow rate ranged from 0.7 to 2.5 kg/min while the gas flow rate ranged from 0.5 to 1.5 kg/min. The water/CO_2 molar ratio was maintained between 6.0 and 8.5 in this study.

Data Analysis Method

Wilson Plot Method. To estimate the heat transfer coefficient on the ribbon-finned coolant side, the Wilson plot method[37] was employed. This is one of several approximate methods[38] for determining the relationship between the temperature difference and the heat flux on either side of a heat exchanger. The Wilson technique relies on the assumption that the three terms on the right-hand side of eq 1 are substantially independent of each other. In reality, the film coefficients themselves are not exactly constant—they depend on the (changing) fluid properties, especially viscosity and the gas volume fraction. Specifically, h_{PF} depends on the process fluid conditions and physical properties of gas, liquid, and solid. Likewise, $k_{W,eff}$ depends on the wall materials and the dimension of the tube and h_C depends on the coolant properties, flow condition, and fin geometry. However, in our studies, conditions were chosen so that the temperature changes of both water and coolant were relatively small, and the fluid properties remain nearly constant. Thus, for constant physical properties, a fixed water and gas flow rate on the tube side, and constant wall thickness and fin geometry/conductivity, the overall over heat transfer coefficient should be solely a function of the coolant flow velocity. Within this approximation, overall heat resistance can be expressed as a function of the coolant velocity:

$$\frac{1}{U_i} = K_1 + K_2 V_C^{-\alpha} \tag{4}$$

where K_1 accounts for the heat transfer resistance from the process fluid and the wall (essentially a combination of the first two individual resistances shown in eq 1), K_2 represents the heat transfer resistance from the coolant side to the fins/wall, and V_C is the velocity of coolant (cm/s). The Wilson plot consists of $1/U_i$ versus $V_C^{-\alpha}$ which should be a straight line with intercept K_1 and slope K_2. In practice, α, K_1, and K_2 are empirically determined from experimental data. In the case of a smooth cylindrical tube wall, the wall resistance can be calculated directly and hence separated from the tube-side resistance. Once the shell side heat transfer coefficient was estimated, it was then used to estimate the tube-side heat transfer coefficient in subsequent experiments involving hydrate production.

Thermal Balance. Figure 2 indicates the flow directions of process fluid and coolant in an individual tail tube section of the CFR. The process fluid—gas, liquid, and solid hydrate—flows horizontally while coolant flows in a counter-current direction on the shell-side. A thermal balance between process fluid and coolant was formulated based on the following assumptions:

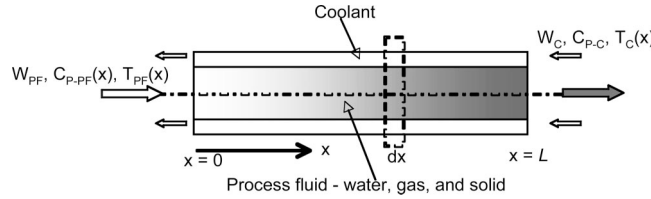

Figure 2. Illustration of fluid directions of process fluid and coolant in a section of the CFR.

(1) Heat losses between the CFR and the surroundings are reflected in the outlet temperature change of coolant. Thus, the heat loss from the process fluid plus the heat uptake from the surroundings equals the heat gained by the coolant.

(2) When the conditioned feedwater is fully saturated with CO_2, the heat generated within the process fluid is due solely to hydrate formation.

(3) Gas, liquid, and hydrate are well mixed and thus have the same temperature within a cross-section of the tail tube. The measured bulk temperature of the process fluid taken at various axial positions is used in the heat balance calculation.

(4) The metal ribbon fins on the shell-side promote effective mixing in the coolant. The outer wall temperature is assumed to be essentially the same as the bulk temperature of coolant. The measured bulk coolant temperature is used in the heat balance calculation.

(5) Due to the high fluid velocity (short residence time within any given tail tube section), it is assumed that heat generation rate due to hydrate formation and the heat transfer coefficient are constant within each individual section of tail tube.

(6) The mechanical heat generation due to the friction among the gas, liquid, and hydrate particles and the frictional heating due to fluid-wall drag are small relative to the heat liberated by hydrate formation and can be neglected.

(7) The inner diameter of the tail tube is constant for the entire tail tube (i.e., slight alterations induced by the thermal and pressure sensing probes carefully positioned at the wall have minimal effect on the effective diameter).

As solid hydrate forms along the tail tube, the physical properties of the mixture change. Therefore a differential form of the steady-state heat balance was deemed appropriate:

$$\frac{dQ_{PF}}{dx} = W_{PF} C_{P-PF} \frac{dT_{PF}(x)}{dx} = -U_{i,x} \pi D_i (T_{PF}(x) - T_C(x)) + Q_H \tag{5-1}$$

$$\frac{dQ_C}{dx} = -W_C C_{P-C} \frac{dT_C(x)}{dx} = U_{i,x} \pi D_i (T_{PF}(x) - T_C(x)) \tag{5-2}$$

$$\frac{dQ_{PF}}{dx} = \frac{dQ_C}{dx} \tag{5-3}$$

where Q denotes the rate of heat transfer (J/s), W is the mass flow rate (g/s), C_p is the effective heat capacity (J/g K), T is bulk temperature (°C), and subscripts C and PF refer to coolant and process fluid, respectively. In these equations, $U_{i,x}$ is the local overall heat transfer coefficient based on the inner area of the tail tube (J/cm^2 s K), and Q_H denotes the hydrate formation heat rate per unit length (J/cm s). If there is no hydrate formation within the tail tube, Q_H is zero. On the other hand, when hydrate formation occurs, the value of Q_H is no longer zero. Then, changes in the coolant temperature are due not only to the

(37) Wilson, E. E. A basis for rational design of heat transfer apparatus. *Trans. ASME* **1915**, *37*, 47–82.

(38) Rose, J. W. Heat-transfer coefficients, Wilson plots and accuracy of thermal measurements. *Exp. Therm. Fluid Sci.* **2003**, *28* (2−3), 77–86.

sensible heat changes in the process fluid temperature but also due to heat liberation during hydrate formation.

Material Balance. The slurry concentration (e.g., mass percent solids) increased as the mixture flowed down the tail tube, and this significantly influenced the multiphase flow pattern. Thus, a means of estimating the fraction of solids was necessary. A coupled heat and material balance was formulated. Specifically, the enthalpy of hydrate formation is known as a function of pressure and temperature,[39] so the rate of hydrate formation in a given section of tail tube can be estimated from the heat liberated:

$$n_{H,i} = \frac{Q_{TH,i}}{\Delta H_{T,P}} \tag{6}$$

where ($\Delta H_{T,P}$) is the hydrate heat-of-formation (J/mol), $n_{H,i}$ is the hydrate formation rate in section i (mol/s), and $Q_{TH,i}$ is the heat generated due to the hydrate formation in section i (J/s). The temperatures of both process fluid and coolant were measured at the entry and inlet of each section of the CFR, thus a heat balance was carried over each individual section. If the ratio of water to CO_2 molecules in the hydrate crystal is denoted as N_H, the slurry concentration at a given point along the tail tube at the steady state can be calculated using

$$C_{slurry,i} = \frac{\sum_1^i n_{H,i} \cdot 44 + \sum_1^i n_{H,i} N_H \cdot 18}{W_{W,feed} + \sum_1^i n_{H,i} \cdot 44} \tag{7}$$

where $C_{slurry,i}$ is the mass concentration of slurry during the hydrate reaction at the exit of section i (mass fraction) and $W_{W,feed}$ is the water feed mass flow rate (g/s). Since the hydration number (N_H) changes with temperature and CO_2 partial pressure,[39] an average temperature for a given section was determined (based on the inlet and outlet temperatures) and used to estimate the appropriate hydration number for that section.

As hydrate formation continued along the tail tube, more CO_2 was taken up by the hydrate phase and thus disappeared from the gas phase (the cumulative amount is given by the summation over $n_{H,i}$). The CO_2 concentration (described as mole fraction) at the exit of each section was calculated as follows:

$$x_{CO_2,off,i} = \frac{(W_{G,feed}/MW_{G,feed})\, x_{CO_2,feed} - \sum_1^i n_{H,i}}{W_{G,feed}/MW_{G,feed} - \sum_1^i n_{H,i}} \tag{8}$$

where $x_{CO_2,off,i}$ is the mole fraction of CO_2 in the gas exiting section i, $W_{G,feed}$ is the mass flow rate of the feed gas (g/s), $MW_{G,feed}$ is the molecular weight of mixed gas (g/mol) in the feed gas, and $x_{CO_2,feed}$ is the mole fraction of CO_2 in the feed gas. Of course, the CO_2 mole fraction at the exit of section i (i.e., $x_{CO_2,off,i}$) equals that at the entry of section $i + 1$ (i.e., $x_{CO_2,in,i+1}$).

Determination of Process Fluid Velocity. The process fluid consisted of gas, liquid, and solid, all of which contribute to the net linear velocity. Since CO_2 and water combine to form the solid phase, mass flow rates of both the gas and liquid phases vary. Knowing the amount of hydrate at each section (from the heat and material balances), allows the changes in mass flow rate for both gas and liquid (containing hydrate) to be tracked using

$$M_{W,i} = M_{W,feed} - \sum_1^i n_{H,i} \cdot N_H \cdot 18 \tag{9-1}$$

$$M_{H,i} = \sum_1^i n_{H,i}(44 + N_H \cdot 18) \tag{9-2}$$

$$M_{G,i} = M_{G,feed} - \sum_1^i n_{H,i} \cdot 44 \tag{9-3}$$

where $M_{W,i}$, $M_{H,i}$, and $M_{G,i}$ are the mass flow rates (g/s) of water, hydrate, and gas phase at the exit of section i, respectively. Their volumetric flow rate can be also determined if the density of each phase is known:

$$Vol_{W,i} = M_{W,i}/d_{W,T,i} \tag{10-1}$$

$$Vol_{H,i} = M_{H,i}/d_{H,T,i} \tag{10-2}$$

$$Vol_{G,i} = M_{G,i}/d_{G,T,P,i} \tag{10-3}$$

where $Vol_{W,i}$, $Vol_{H,i}$, and $Vol_{G,i}$ are the total volumetric flow rates (cm^3/s) of water, hydrate, and gas phases at the exit of section i, respectively. The densities (g/cm^3) of the water, hydrate, and gas phases at the exit of section i are denoted as $d_{W,T,i}$, $d_{H,T,i}$, and $d_{G,T,P,i}$, respectively. A hydrate phase density of 1.12 g/cm^3 was used in the calculations.[40]

The average temperature (and pressure) measured at the entry and exit of each tail tube section was used to calculate the physical properties of gas phase for that section. The physical properties of pure gas (CO_2, Ar, or He) and water were obtained from the NIST vapor/liquid phase database (http://webbook.nist.gov/chemistry/fluid). A mole fraction weighted mixing rule was used to determine the physical properties for the gas mixtures. More specifically, the density of the gas mixture was calculated as follows:

$$d_{G,T,P,i} = \left(x_{CO_2,i} d_{CO_2,T,P,i}/44 + (1 - x_{CO_2,i}) d_{inert,T,P,i}/MW_{inert}\right) MW_{G,i} \tag{11-1}$$

$$x_{CO_2,i} = \frac{x_{CO_2,in,i} + x_{CO_2,off,i}}{2} \tag{11-2}$$

$$MW_{G,i} = 44 x_{CO_2,i} + MW_{inert}(1 - x_{CO_2,i}) \tag{11-3}$$

$$\text{for Ar, } MW_{inert} = 40 \text{ for He, } MW_{inert} = 4 \tag{11-4}$$

where $d_{CO_2,T,P,i}$ and $d_{inert,T,P,i}$ are the density of pure CO_2 and inert gas (either Ar or He) at T and P, respectively. $MW_{G,i}$ is the average molecular weight of mixed gas at section i (g/mol).

Since the total volumetric flow rate is the sum of the volumetric flow rate of the different phases, the superficial velocity of the process fluid can be calculated using

$$Vol_{T,i} = Vol_{W,i} + Vol_{H,i} + Vol_{G,i} \qquad V_{PF,i} = \frac{Vol_{T,i}}{A_T} \tag{12}$$

(39) Anderson, G. K. Enthalpy of dissociation and hydration number of carbon dioxide hydrate from the Clapeyron equation. *J. Chem. Thermodyn.* **2003**, *35* (7), 1171–1183.

(40) Udachin, K. A.; Ratcliffe, C. I.; Ripmeester, J. A. Structure, composition, and thermal expansion of CO2 hydrate from single crystal X-ray diffraction measurements. *J. Phys. Chem. B* **2001**, *105* (19), 4200–4204.

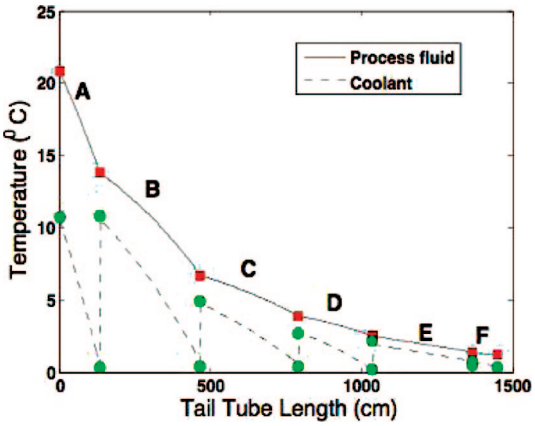

Figure 3. Temperature profiles along the tail tube (in this specific run, water = 1500 g/min, N_2 = 130 g/min, and coolant flow rate = 1.5 cm/s). The letters A−F indicate sequential tail tube sections with A being closest to the venturi mixer, the squares are measured temperatures for the process fluid, and the circles are experimental points for coolant inlet and outlet. Recall that within each section, the coolant flow is countercurrent to the process fluid, thus the coolant inlet temperature is roughly zero (i.e., the set point) and increases within each section. The connecting lines between the circles were obtained by solving the differential thermal balance equations.

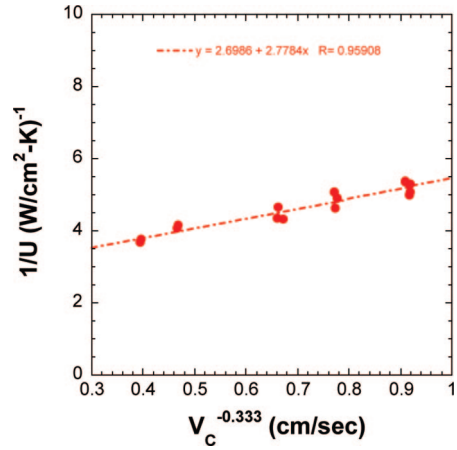

Figure 4. Wilson plot for the three sections of tail tube (for these data, the water flow rate was 1500 g/min, gas mass flow rate was 110 g/min, average pressure was ~110 psia, and at ambient temperature, the process fluid velocity was >5.0 m/s).

where $V_{PF,i}$ is the superficial velocity of the process fluid at the exit of section i (cm/s) and A_T is the inner cross-sectional area of the tail tube (cm^2).

A computer program developed using MathWork software was used to calculate the overall heat transfer coefficient, volume fraction, fluid superficial velocity, slurry concentration, and CO_2 concentration and to solve the coupled heat and material balances. To lessen the effects of fluctuations inherent in the experimental data, the temperature, pressure, and mass flow rate used in the calculations were an average of those measured during the steady-state operational period over which data was collected. Data points were typically collected over a 5−10 min interval.

Results and Discussion

Thermal Losses. Although the CFR system was well-insulated, there was heat exchanged between the CFR and the surroundings. It proved largest when the coolant temperature setting was below zero and the coolant velocity was slow (<5 cm/s). The heat exchange was quantified at different coolant velocities while the interior CFR tube was filled with still air. The temperature gain in the coolant was ~0.7 °C in the longest section (~4 m long) when the coolant velocity was the lowest (1.5 cm/s) and the coolant temperature setting was lowest (−3.5 °C). The temperature gain in the shortest section (~1 m long) was not appreciable (~0 °C) when the coolant velocity was high (>5 cm/s) and the temperature setting was above zero. Since losses varied from section-to-section, a separate correction was developed and used in heat balance calculations for each individual tail tube section.

Coolant (Shell-) Side Heat Transfer Coefficient (h_C). Thermal measurements were made using tube-side flow conditions similar to that used in the hydrate production. A nitrogen−water mixture was used at gas−liquid flow ratios similar to the hydrate formation runs. This mixture resulted in multiphase (gas−liquid) flow but avoided the heat generation associated with hydrate production.

Figure 3 illustrates typical temperature profiles when nitrogen and water were used in reactor configuration one. In this specific run, ambient temperature nitrogen and water were fed into the tail tube while the shell-side coolant (whose inlet temperature set at 0 °C) flowed countercurrent through each individual section. When the process fluid reached the end of the tail tube assembly, its temperature approached the coolant temperature even when the coolant velocity was less than 3.0 cm/s. Consequently, the temperature change on the coolant side became very small (<0.3 °C) in those downstream sections. Since the accuracy of temperature sensors was ±0.1 °C, such a small temperature difference can potentially lead to a large experimental error. In a similar vein, entry effects associated with the venturi mixer and in establishing of the flow regime may result in unique dynamics (i.e., "entry" effects) in the first section (section A). Thus, thermal data from sections A, E, and F were omitted while data from sections B−D were used for analysis.

The overall heat transfer coefficient was estimated by varying the coolant flow rates (in this case from 1.5 to 15 cm/s) with fixed N_2/water flow rates. The thermal data collected from sections B, C, and D were used to construct the Wilson plot shown in Figure 4.

The empirically determined parameters K_1 and K_2 in eq 4 were found to be 2.70 and 2.78, respectively. The correlation between the heat transfer coefficients (h_C) of the coolant side (W/cm^2 s) and the coolant velocity (V_C, cm/s) is thus

$$h_C = 0.36 V_C^{0.333} \tag{13}$$

Since all of the tail tubes sections were manufactured by the same company and are of identical design, very similar overall heat transfer coefficients were obtained for each section. Hence, it was assumed that this correlation is valid for all sections in both CFR configurations. This is reasonable provided that operational conditions (coolant flow rate and temperature difference between coolant and process fluid) remain within the ranges used to develop the correlation.

Operational Stability. Hydrates are well-known in gas transmission as the source of pipeline plugs. Thus, plugging was a general concern in the operation of the CFR system. In an early design, where the inner diameter of the tail tube was ~0.5 cm, intermittent plugging was an issue. This was especially true when the shell-side coolant temperature was low and hydrate formation was very rapid. However, once the inner diameter of the tail tube was increased to 0.8 cm, the plugging issue became far less common provided the fluid velocity was high enough to maintain turbulent flow conditions and the coolant temperature/flow was

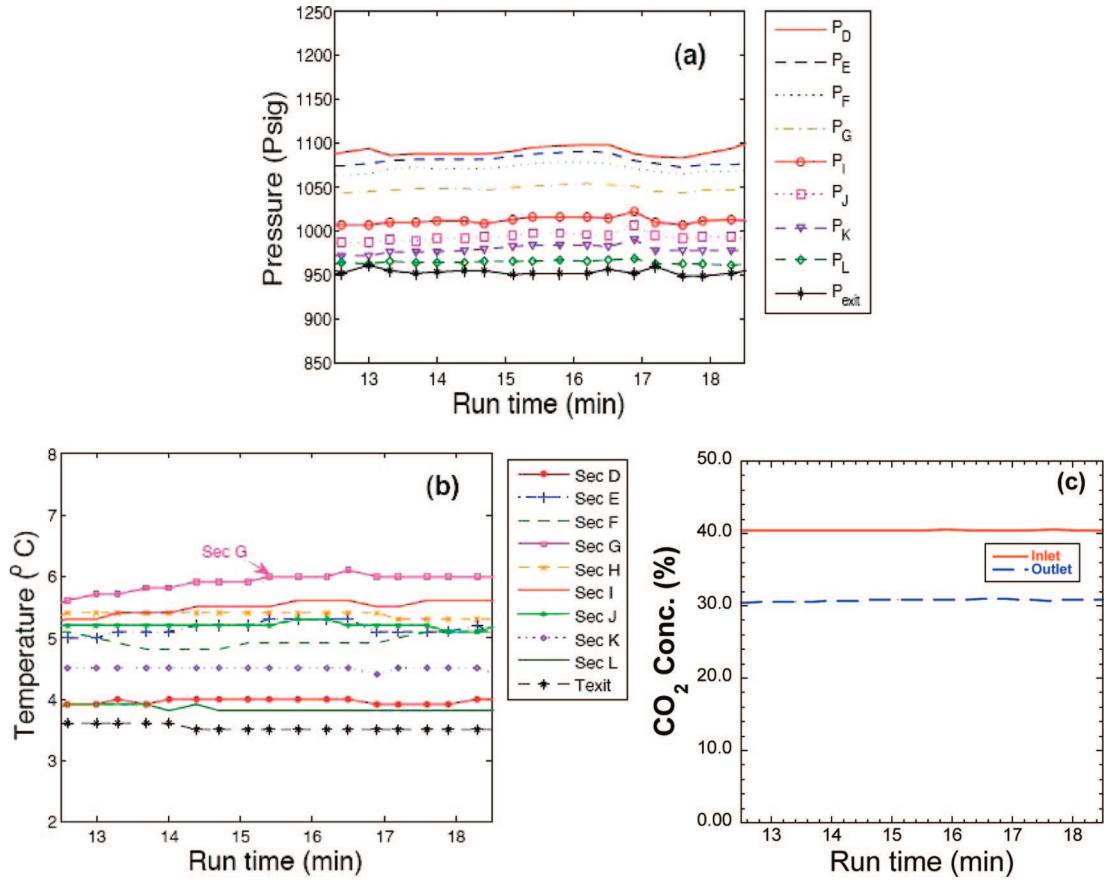

Figure 5. Process fluid profiles in tail tube sections D−L: (a) pressure, (b) process fluid temperature, and (c) CO_2 concentration at the inlet and outlet of the tail tube. Data are from a He/CO_2 hydrate production run using reactor configuration two (both pressure and temperature readings are made at the entry to the specific tail tube section).

controlled so that hydrate formation was more uniform along the tail tube. Stable runs lasting more than 40 min were reproducible (this time corresponds to near consumption of the saturated water supply). However, to facilitate data acquisition over a wide range of conditions, one set of test conditions was typically maintained at steady state for about 5−10 min and then changed to another set of interest. Figure 5 shows typical traces for (a) pressure changes along the CFR, (b) temperature changes of the process fluid along the CFR, and (c) CO_2 concentration at the inlet and outlet of the CFR. These data are from a steady-state period of a He/CO_2 hydrate experiment. In this particular experiment, the water/CO_2 molar ratio was controlled to ~7.25. At the highest superficial velocity, the pressure drop across the entire CFR is less than 150 psi. However, as the process flow rate was decreased, the pressure drop could increase up to as much as 250 psi. High velocity was found to contribute to stable operation. In general, 25−40% of the CO_2 was removed from the CFR. For the particular run shown in Figure 5, about 10% of the CO_2 concentration decreased in the outlet gas, which was equivalent to 36% CO_2 removal from the feed gas (see Figure 5c).

Due to appreciable hydrate formation, a large amount of heat was typically generated in the CFR resulting in a higher process fluid exit temperature (Figure 5b). To ensure continued hydrate formation along the tail tube, the heat of formation must be effectively removed by using the available heat transfer mechanisms. In the following sections, we focus attention on those heat transfer processes during hydrate formation. Details related to the associated kinetics and hydrodynamics of continuous hydrate formation will be addressed in a separate communication.

Heat Transfer with Hydrate Formation. The formation of hydrate from water and CO_2 is exothermic. As a result of changes in cage occupancy, the hydrate heat-of-formation varies from 63 to 58 KJ/mol as the temperature changes from 1 to 9 °C.[39] Due to the large sensitivity to both temperature and pressure,[8,15,32,41] the global hydrate formation rate will be affected by heat transfer processes. Also, the water/CO_2 molar ratio can have a significant impact on the gas volume fraction, flow pattern, slurry concentration, and hence the observed hydrate formation rate. The water/CO_2 molar ratio was typically controlled between 6.5 and 8.0 in this study unless otherwise indicated. Heat transfer results presented below were collected using both reactor configurations. The process fluid velocity used in configuration two (~22.5 m) was typical higher than that used in configuration one (~14.5 m). In all cases, hydrate typically formed rapidly in the front sections due to a large initial driving force. The heat generated as a result of that hydrate formation caused the temperature of the process fluid to initially increase rapidly. Subsequently, as the hydrate formation rate decreased and heat was continually removed from the process fluid, the temperature of the process fluid gradually decreased in the later sections.

For known flow rates and inlet/outlet temperatures for the process fluid and coolant, the differential forms given in eqs 5 were solved numerically to determine the overall heat transfer coefficient for each section. The overall heat transfer coefficients given in eqs 5 were estimated using the inlet temperatures and best fitting the measured outlet temperatures of both process fluid and coolant. With the estimated overall heat transfer coefficient, the temperature profiles of process fluid and

(41) Uchida, T.; Ebinuma, T.; Narita, H. Observations of CO2-hydrate decomposition and reformation processes. *J. Cryst. Growth* **2000**, *217* (1/2), 189–200.

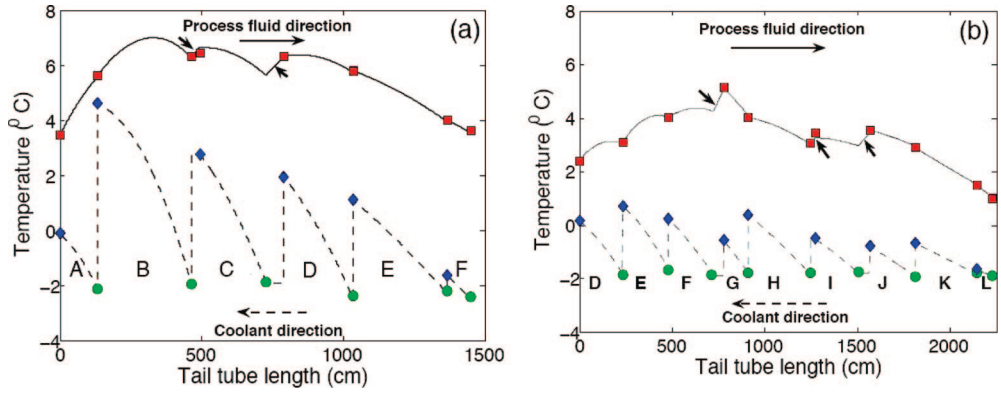

Figure 6. Temperature profiles of process fluid and coolant obtained from a typical hydrate run in configuration one (a) and in configuration two (b). Letters again indicate the various tail tube sections; square symbols are experimental points for the process fluid; circular and diamond symbols are experimental points for the coolant inlet and outlet, respectively. Note that within each tail tube section, the coolant flow is countercurrent to the process fluid. Thus, the coolant inlet temperature in each section is roughly the same (i.e., at the set point) and increases in each section. There were short insulated tail tube sections without active cooling (e.g., for viewing ports). As a result, the temperature rose slightly in these sections. The arrows in these plots indicated the short sections without active cooling.

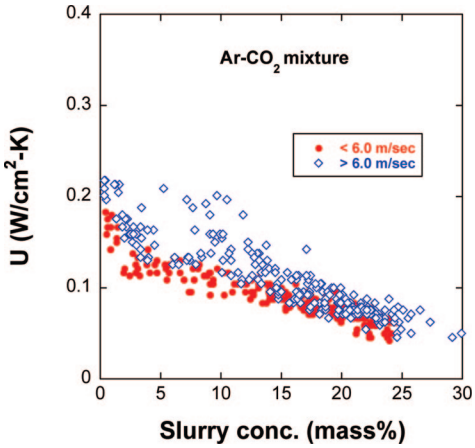

Figure 7. Estimates of overall heat transfer coefficient vs slurry concentration obtained from the Ar/CO_2 runs under hydrate formation conditions (coolant velocity = 5.0−7.5 cm/s).

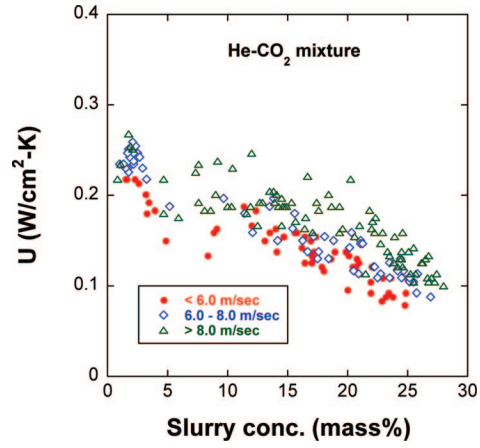

Figure 8. Estimates of overall heat transfer coefficient vs slurry concentration obtained from the He/CO_2 runs (coolant velocity = 5.0−7.5 cm/s). Multiphase flow regimes were similar to those observed in the comparable Ar/CO_2 experiments.

coolant along the CFR were then calculated. Typical temperature profiles calculated for both process fluid and coolant are shown in Figure 6.

A plot of the overall heat transfer coefficient (U) verses slurry concentration from the Ar/CO_2 experiments is shown in Figure 7. With increasing slurry concentration, a trend of decreasing U was observed. When water and gas were first mixed in the venturi, very effective heat transfer took place (but the slurry concentration was typically less than 5 mass %). The good interphase mixing and the low solid concentration suggest a high U. Thus, the process fluid superficial velocity had appreciable impact on U in these first sections.

However, when the slurry concentration was higher than 15 mass %, the effect of velocity was found to be less pronounced. The slurry concentration appeared to have more impact on the process-side heat transfer process. Two factors may contribute to the reduction in heat transfer efficiency. First, a change in the multiphase flow pattern is expected as the slurry concentration increases. Second, a decreasing temperature difference exists between the coolant and the process fluid as the latter travels down the tail tube (a decreased thermal diving force).

In the typical hydrate experiment, an annular flow pattern was observed in the first (upstream) view port. Due to gravity, the liquid film at the top portion of tube is usually thinner than that at the bottom in a horizontal tube in gas−liquid annular flow.[34] The liquid layer coating the tail tube may be critical to heat transfer since the thermal conductivity of water was about 25−35 times higher than that of the gas phase. Although the velocity had some impact, the high thermal conductivity of water is likely key for effective heat transfer in the front sections. The annular flow pattern usually disappeared by the second view port, mounted at the exit of the tail tube. In the down stream sections, the liquid and solid phases formed strips of ice-like slush that appeared to be in a slug flow regime. The hydrate density (1.12 g/cm^3) is higher than that of water[40] and thus might be expected to settle. It was also observed that the hydrate particles tended to aggregate and include interstitial water. Thus, the poorer heat transfer observed in the downstream sections may be due to more portions of the tube surface now being exposed to the lower conductivity gas phase. In such a case, the thermal conductivity of the gas becomes an important factor in determining the overall heat transfer rate.

The effect of slurry concentration and fluid superficial velocity on U for the He/CO_2 runs is shown in Figure 8. In general, the overall heat transfer coefficient obtained from the He/CO_2 mixture was higher than that obtained from the Ar/CO_2 mixture at similar flow conditions. This is likely due to the higher thermal conductivity of Helium relative to Argon. However, the difference in U between these two gas mixtures was not significant in the first sections of tail tube. This suggests again that the high thermal conductivity of water dominates heat transfer in the front sections of tail tube. However, when slurry concentration was higher than 10−15 mass %, differences in

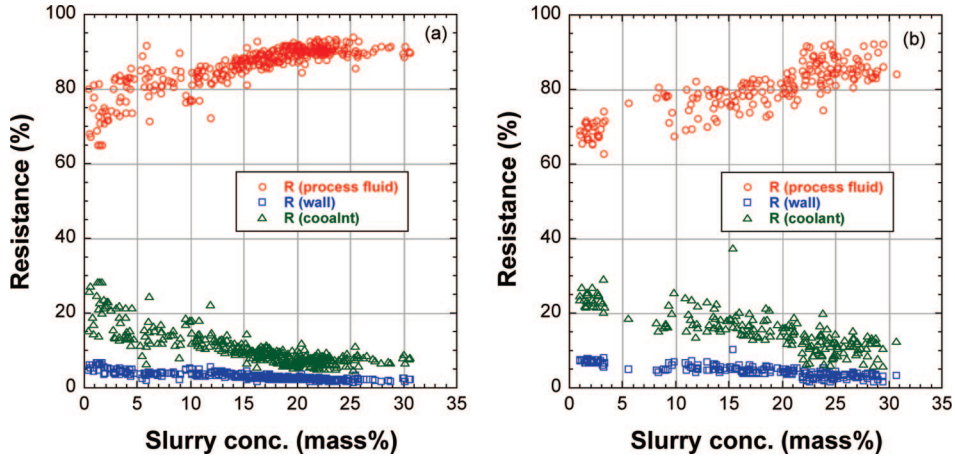

Figure 9. Illustration of resistance contribution based on the experimental results (a) for Ar/CO_2 system and (b) for the He/CO_2 system (process fluid velocity ranges from 4−8 m/s and coolant velocity ranges from 5.0−7.5 cm/s).

the heat transfer coefficients between the two gas mixtures became more apparent. The overall heat transfer coefficient decreased at the later sections in the He/CO_2 runs, but did not decrease nearly as much as observed in the Ar/CO_2 runs. These results suggest that the properties of the gas become important in the later sections. Due to the high thermal conductivity of He (≥8 times higher than that of Ar), the overall heat transfer coefficient obtained in the He/CO_2 runs is appreciably higher than that obtained from the Ar/CO_2 gas mixture in the downstream sections of the tail tube. When the velocity of the process fluid increased above 8 m/s, the annular flow pattern was preserved further down the tail tube. The comparison between the Ar/CO_2 and the He/CO_2 runs suggests that even higher heat transfer coefficients should be expected for a syngas system since the thermal conductivity of H_2 is even higher than that of He. Higher flow velocities would be used in industrial practice as well.

Argon has been reported to form hydrates under much higher pressure (>5000 psia at 273 K).[42–45] In comparison, CO_2 hydrates forms 188.5 psia at 273.6 K.[15] Still, there exists the possibility that some argon is incorporated into the hydrate phase along with the CO_2 (with CO_2 essentially acting as the "help gas" for argon-containing hydrate formation).[42] However, over the operational pressure range employed in this study (<1350 psia), we could not detect argon in the gas discharged from the flash reactor, which was generated by decomposing the hydrates. On the other hand, helium is an inert gas that does not form hydrate. Thus, the He/CO_2 mixture is a more representative surrogate for shifted synthesis gas (predominantly a H_2/CO_2 mixture). Quantitative comparisons were made between He/CO_2 and H_2/CO_2 in a bench-scale flow reactor which showed that He was an adequate surrogate for H_2.[14]

As the slurry concentration increases during high fluid velocity experiments that maintain turbulent flow conditions, frictional heating due to fluid-wall drag can be expected to increase. Such heat generation may ultimately become appreciable enough to alter the heat balance and thus impact the deduced hydrate production rate. However, based on the experimental data in Figure 5, if we assume that all of the $P-V$ work is converted into frictional heat, this amount energy is still less than 6.5% of total heat removed from the CFR. Also, the agreement between the experimental CO_2 concentration in the exhaust gas (obtained from GC measurements) and the calculated results (derived from heat balance) was very good. Therefore, in analyzing the current CFR configurations we did not include a frictional heat generation term in the heat balance. Of course, for very long reactors with high fluid velocities, a more detailed energy balance should be formulated to account for frictional heat generation.

As pointed out above, the decrease in overall heat transfer coefficient in the later sections of the tail tube may be also due in part to a lower temperature difference between process fluid and coolant. A single chiller unit was dedicated to the entire tail tube and the coolant inlet temperature was virtually the same at each section of tail tube. A separate cooling system, with independent temperature settings, should improve heat transfer in the downstream sections.

Heat Transfer Resistances. The heat transfer coefficient of the coolant side (h_C) was estimated using the Wilson plot and the overall heat transfer coefficients by direct measurements of temperature gains in coolant and process fluid. If one assumes the heat transfer resistance of the tail tube wall can be calculated based on the known conductivity of 304 stainless-steel ($k_{W,eff}$), then the effective heat transfer coefficient of the process fluid side (h_{PF}) can be back-calculated using eq 1. Figure 9a shows the resistances in the Ar/CO_2 runs. The major heat transfer resistance (>60%) was from the process fluid side. When the slurry concentration was higher than 10 mass %, the resistance from the process fluid side was even larger (>80%). When Ar was replaced by He, the resistance from the process fluid side decreased about 5−10% (see Figure 9b). Due to the higher thermal conductivity of He, the overall heat transfer coefficients in the He/CO_2 system were as much as 50−200% higher than those observed in the Ar/CO_2 system under similar conditions. The benefit of a high thermal conductivity gas is clear.

Figure 10 shows the effect of process fluid velocity on the heat transfer resistance associated with the process fluid side (He/CO_2 experimental results). As the superficial velocity of the process fluid increased from 6.0 to higher than 8.0 m/s, the resistance from the process fluid decreased 10−15%. This

(42) Halpern, Y.; Thieu, V.; Henning, R. W.; Wang, X. P.; Schultz, A. J. Time-resolved in situ neutron diffraction studies of gas hydrate: Transformation of structure II (sII) to structure I (sI). *J. Am. Chem. Soc.* **2001**, *123* (51), 12826–12831.

(43) Shimizu, H.; Tada, N.; Ikawa, R.; Kume, T.; Sasaki, S. Optical microscopy and in situ raman scattering of single crystalline ethylene hydrate and binary methane-ethylene hydrate at high pressures. *J. Phys. Chem. B* **2005**, *109* (47), 22285–22289.

(44) Shimizu, H.; Hori, S.; Kume, T.; Sasaki, S. Optical microscopy and Raman scattering of a single crystalline argon hydrate at high pressures. *Chem. Phys. Lett.* **2003**, *368* (1/2), 132–8.

(45) Suwa, I.; Kato, T.; Sasaki, S.; Shimizu, H. High-pressure Brillouin scattering study on Ar hydrate. *J. Phys.: Condens. Matter* **2002**, *14* (44), 10679–82.

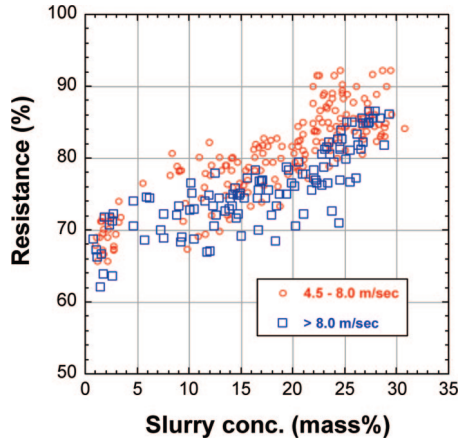

Figure 10. Effect of process fluid superficial velocity on the resistance of heat transfer from the process fluid side for the He/CO_2 system (coolant velocity = 5.0−7.5 cm/s).

decrease can be attributed to vigorous turbulence creating a well-mixed combination of water, gas, and hydrate. Therefore, to reduce the heat transfer resistance on the process fluid side, increasing the fluid velocity and using a carrier gas with a high thermal conductivity both would be beneficial. Industrial designs for the SIMTECHE process involve higher thermal conductivity hydrogen as a carrier gas (i.e., shifted synthesis gas) and will also likely employ higher linear flow velocities.

Conclusions

In this work, the formation of CO_2 gas hydrates from water and gas has been investigated in a continuous flow reactor, using both Ar/CO_2 and He/CO_2 mixtures. Key heat transfer issues were explored using high fluid velocities and high gas volume fractions. The effects of fluid velocities, carrier gas, and slurry concentration on the heat transfer process were interrogated. As one might expect, high fluid velocity enhances mixing among gas, liquid, and solid phases, and thus improves the heat transfer efficiency.

Annular flow patterns were observed in the early sections of the reactor where a thin liquid film coated the inner wall. In this regime, the thermal conductivity of the water appeared to dominate the heat transfer coefficient on the process fluid side. However, as more and more solid hydrate formed, the change in density together with hydrate precipitation at the bottom of the tail tube induced a change in the multiphase flow pattern. The pattern gradually evolved from annular flow to slug flow when the hydrate concentration became greater than 15 mass %. In the resulting slug flow regime, more of the tail tube is likely exposed directly to the gas phase. In this regime, the heat transfer coefficient then appeared to be more sensitive to the thermal conductivity of the carrier gas. It was shown that a carrier gas with a high thermal conductivity enhanced the heat transfer process significantly once appreciable amounts of hydrate was formed. Specifically, when Ar was replaced with He as the carrier gas, the overall heat transfer coefficient increased about from 50−200% under similar fluid flow conditions. These differences between He and Ar suggest that even better heat transfer should be expected from a shifted synthesis gas mixture, which typically contains more than 55% H_2. A higher fluid velocity appeared to help preserve an annular flow pattern, which is beneficial to heat transfer from the multiphase mixture. This study provides some important engineering information related to the CO_2 hydrate formation in continuous flow reactors that can be used in future designs and demonstrations of this promising hydrate-based CO_2 capture process.

Acknowledgment. The authors wish to thank Graydon Anderson, Stephen Obrey, and King Ng for many fruitful suggestions and discussions. Expert mechanical assistance from Michael Sedillo in building the ETM system is also acknowledged. This work was funded by the US Department of Energy (Office of Fossil Energy), for which the authors are grateful.

EF700749F